Nonlin. Processes Geophys. Discuss., doi:10.5194/npg-2016-81, 2016
Manuscript under review for journal Nonlin. Processes Geophys.
Published: 14 December 2016
© Author(s) 2016. CC-BY 3.0 License.

Nonlinear Processes in Geophysics
Discussions
Open Access
EGU

# A Simple Kinematic Model for the Lagrangian Description of Relevant Nonlinear Processes in the Stratospheric Polar Vortex

Victor José García-Garrido[1], Jezabel Curbelo[1,2], Carlos Rorberto Mechoso[3], Ana María Mancho[1], and Stephen Wiggins[4]

[1]Instituto de Ciencias Matemáticas, CSIC-UAM-UC3M-UCM. C/ Nicolás Cabrera 15, Campus de Cantoblanco UAM, 28049 Madrid, Spain.
[2]Departamento de Matemáticas, Facultad de Ciencias, Universidad Autonóma de Madrid, 28049 Madrid, Spain.
[3]Department of Atmospheric and Oceanic Sciences, University of California at Los Angeles, Los Angeles, California.
[4]School of Mathematics, University of Bristol. Bristol BS8 1TW, UK.

*Correspondence to:* A. M. Mancho (a.m.mancho@icmat.es)

**Abstract.** In this work we study the Lagrangian footprint of the planetary waves present in the Southern Hemisphere stratosphere during the Sudden Stratospheric Warming event that took place during September 2002. The Lagrangian analysis of the transport and mixing processes is carried out in the framework of dynamical systems theory, by means of a Lagrangian descriptor. We seek to describe the Lagrangian skeleton of geometrical structures that lead to filamentation phenomena and the breakdown of the polar vortex, and establish its relation with how planetary waves interact. Our approach is based on the construction of a simple kinematic model, inspired by the Fourier decomposition of the geopotential field. We show that this model is capable of reproducing the key Lagrangian features present on the reanalysis data such as the formation of filaments eroding the stratospheric polar vortex and the breakdown of the vortex.

## 1 Introduction

A better understanding of the behavior of fluid parcels is of fundamental importance for studies on the dynamics and chemistry of the stratosphere. This was dramatically demonstrated by the intense research effort that followed the discovery of the "Antarctic Ozone Hole" phenomenon in the 1970's. Following decades during which monitoring of ozone in atmospheric columns above Antarctica showed little interannual variability, in situ measurements corroborated by satellite data, revealed that ozone was systematically decreasing in the Antarctic lower stratosphere during the southern spring season. Whilst this was immediately associated with the simultaneous increase in atmospheric pollution by anthropogenic activities, several key questions arose: 1) Why over Antarctica and not over the Arctic since pollution sources are stronger in the northern than in the southern hemisphere? 2) Why in the spring season? and 3) Will ozone depletion extend worldwide? The research demonstrated that indeed increased atmospheric pollution was to be blamed for the ozone depletion and identified the participating substances and special mechanisms. The research also demonstrated that the unique atmospheric conditions above Antarctica were responsible for the geographic preference for ozone destruction. In particular, it was shown that the strong circumpolar and westerly flow characteristic of the southern winter and spring stratosphere (hereafter stratospheric polar night vortex,

Nonlin. Processes Geophys. Discuss., doi:10.5194/npg-2016-81, 2016
Manuscript under review for journal Nonlin. Processes Geophys.
Published: 14 December 2016
© Author(s) 2016. CC-BY 3.0 License.

Nonlinear Processes in Geophysics
Discussions
Open Access
EGU

SPV) contributed to isolate the cold polar region setting up a favorable environment for the special chemistry to act. The new knowledge led to the formulation of international agreements that resulted in a negative answer to question 3) above.

Outside the region isolated by the SPV, research also showed strong stirring and mixing of the flow. In this "surf zone" (McIntyre and Palmer, 1984) air parcels can travel long distances away from the SPV in an environment where contours of long-lived tracers such as potential vorticity can stretch forming complex patterns. In this region, which is referred as the "surf zone", Rossby wave breaking is associated with irreversible deformation that pulls material filaments of the outer edge of the SPV and enhances mixing with the exterior flow (McIntyre and Palmer, 1983, 1984, 1985). Such a process makes the SPV edge a barrier to horizontal transport of air parcels (Juckes and McIntyre, 1987) while continuously eroding and regenerating the SPV edge by filamentation (Bowman, 1993). Polvani and Plumb (1992) and Nakamura and Plumb (1994) examined in an idealized setting the way in which Rossby waves break ejecting SPV material outward. The latter conceived a similar setting in which Rossby waves break also inwards.

Dynamical systems theory applies tools that provide valuable insights for describing this type of behavior in fluid flows. Such tools include the geometrical structures referred to as hyperbolic trajectories (HTs), their stable and unstable manifolds and their intersection in homoclinic and heteroclinic trajectories that provide the theoretical and computational basis for describing the filamentation process. Mancho *et al.* (2006b) discussed the possibility of "transferring" this approach to realistic ocean flows produced by models. Bowman (2006) pioneered a similar effort for the stratosphere. de la Cámara *et al.* (2013) suggested that HTs are representative of cat's eye structures associated with planetary wave breaking at the critical levels, i. e. where the wave phase speed matches the background velocity (Stewartson, 1977; Warn and Warn, 1978). HTs are at the locations where the cats eyelids meet. Perturbation of the cat's-eyes results in irreversible deformation of material contours, signifying Rossby wave breaking. de la Cámara *et al.* (2013) and Guha *et al.* (2016) identified HTs both within and without the SPV, thus suggesting that Rossby wave breaking can occur in either of those regions. The former authors worked with reanalysis data, while Guha *et al.* (2016) used a dynamical model based on the shallow water equations in which the perturbing waves are produced in a controlled manner. Therefore, HTs are essential features for tracer mixing both outside and inside the vortex, and for occasional air crossings of the vortex edge.

Our goal in the present paper is to identify essential features in the filamentation process associated with the breakdown of the SPV during a major stratospheric sudden warming. We focus on the warming event that occurred in the southern stratosphere during September 2002. In this unusual event, the SPV broke down in the middle stratosphere (Mechoso *et al.*, 1988; Manney *et al.*, 2006; Charlton *et al.*, 2006). On the basis of reanalysis data and the application of a Lagrangian descriptor (LD) known as the function $M$ we identify key Lagrangian features of the flow. Next we build a kinematic model of the event in order to gain insights on the transport processes occurring in the SPV. Typically kinematic models have provided a simple approach for studying Lagrangian transport and exchange associated with flow structures such as meandering jets and travelling waves (Bower, 1991; Samelson, 1992; Malhotra and Wiggins, 1998; Samelson and Wiggins, 2006). Other works have used simple kinematic models to illustrate phenomena in planetary atmospheres (e.g., Rypina *et al.* (2007); Morales-Juberías *et al.* (2015)). Our kinematic model is constructed to emulate the behavior of planetary waves as obtained from the reanalysis data. We show

Nonlin. Processes Geophys. Discuss., doi:10.5194/npg-2016-81, 2016
Manuscript under review for journal Nonlin. Processes Geophys.
Published: 14 December 2016
© Author(s) 2016. CC-BY 3.0 License.

Nonlinear Processes in Geophysics Discussions
Open Access
EGU

that our model produces strikingly similar transport features to those found in the reanalysis data confirming the key role played by the HTs during vortex breakdown and filamentation.

The structure of the paper is as follows. Section 2 describes the data and methods used in our analysis. Section 3 describes the identified propagating waves in the reanalysis data in the year 2002 in the stratosphere at some specific pressure levels (10hPa) and these are related to filamentation phenomena and the polar vortex breakdown that occurred this year. Section 4 reproduces the findings in an ad hoc analytical kinematical model confirming the role played by the HTs in the 2002 vortex breakdown. Section 5 discusses the consistency of the kinematic model as representative of atmospheric flows that conserve potential vorticity. Finally in section 6 we present the conclusions.

## 2 Data and Methods

### 2.1 ERA-Interim Reanalysis Data

To achieve a realistic representation of the atmospheric transport processes, it is crucial to use a reliable and high-quality dataset. We use in this work the ERA-Interim reanalysis dataset produced by a weather forecast assimilation system developed by the European Centre for Medium-Range Weather Forecasts (ECMWF; Simmons *et al.* (2007)). de la Cámara *et al.* (2013) obtained encouraging results on the suitability of the ERA-Interim dataset for Lagrangian studies of stratospheric motions in their comparison of parcel trajectories on the 475 K isentropic surface (around 20 km) using this dataset and the trajectories of superpressure balloons released from Antarctica by the VORCORE project during the spring of 2005 (Rabier *et al.*, 2010).

The Era-Interim data is available four times daily (00:00 06:00 12:00 18:00 UTC), with a horizontal resolution of $1^\circ \times 1^\circ$ in longitude and latitude and 60 sigma levels in the vertical from 1000 to 0.1 hPa. The data covers the period from 1979 to the present day (Dee *et al.*, 2011) and it can be downloaded from http://apps.ecmwf.int/datasets/data/interim-full-daily/levtype=sfc/. In particular we will use the data for the geopotential height and wind fieldson surfaces of constant pressure for the period August-September 2002. The geopotential height $Z$ on constant pressure surfaces $p$ is defined as the normalization to $g_0 = 9.80665\, ms^{-2}$ (standard gravity at mean sea level) of the gravitational potential energy per unit mass at an elevation $s$ (over the Earth's surface), and has the form:

$$Z(\lambda,\phi,p,t) = \frac{1}{g_0} \int_0^{s(p,t)} g\,(\lambda,\phi,z)\; dz\;, \tag{1}$$

where $g$ is the acceleration due to gravity, $\lambda$ is longitude, $\phi$ is latitude and $z$ is the geometric height (Holton (2004)).

For the analysis of planetary waves, we apply a zonal Fourier decomposition of the geopotential height field on the 10 hPa pressure level (approximately 850 K potential temperature). The zonal wave decomposition yields:

$$Z = \mathcal{Z}_0\,(\phi,p,t) + \sum_{k=1}^{\infty} \mathcal{Z}_k\,(\lambda,\phi,p,t)\;. \tag{2}$$

Nonlin. Processes Geophys. Discuss., doi:10.5194/npg-2016-81, 2016
Manuscript under review for journal Nonlin. Processes Geophys.
Published: 14 December 2016
© Author(s) 2016. CC-BY 3.0 License.



The mean flow is defined as:

$$\mathcal{Z}_0(\phi,p,t) = \frac{1}{2\pi}\int_0^{2\pi} Z(\lambda,\phi,p,t)\; d\lambda\,, \tag{3}$$

and the different modes $\mathcal{Z}_k$ with wavenumber $k \geq 1$ have the sinusoidal description:

$$\mathcal{Z}_k(\lambda,\phi,p,t) = \mathcal{B}_k(\phi,t)\cos\left(k\lambda + \varphi_k(\phi,p,t)\right) \tag{4}$$

where $\lambda \in [0, 2\pi)$ is longitude, $\phi \in [-\pi/2, \pi/2]$ is latitude, $\mathcal{B}_k$ is the amplitude of the wave and $\varphi_k$ its phase. During the warming event occurred in the southern stratosphere during September 2002 the flow was dominated by the contributions of the mean flow and the two longest planetary waves ($\mathcal{Z}_1$ and $\mathcal{Z}_2$; Krüger *et al.* (2005))

### 2.2 Lagrangian Descriptors

The theory of dynamical systems provides an ideal framework for analyzing nonlinear transport and mixing processes that take place in the stratospheric polar vortex by means of Lagrangian techniques. One of the main goals of dynamical systems theory is the qualitative description of the evolution of particle trajectories by means of geometrical objects that partition the phase space (the atmosphere in our case) into regions in which the system shows distinct dynamical behaviors. These geometrical structures act as material barriers to fluid parcels and are closely related to flow regions known as hyperbolic, where rapid contraction and expansion takes place. This methodology has become a cornerstone on the applications of the qualitative theory of dynamical systems to geophysical fluids.

Several Lagrangian techniques have been developed in order to describe the Lagrangian coherent structures (LCS) that comprise the skeleton of the flow and govern transport and mixing in geophysical fluids. The search for such structures in geophysical contexts is challenging because in these contexts the velocity fields are generally aperiodic in time, time-dependent and defined over a discrete space-time domain. Among others the developed techniques include finite-size Lyapunov exponents (FSLE) (Aurell *et al.*, 1997), finite-time Lyapunov exponents (FTLE) (cf. Haller (2000); Haller and Yuan (2000); Haller (2001); Shadden *et al.* (2005)). The techniques also include distinguished hyperbolic trajectories (DHT) (Ide *et al.*, 2002; Ju *et al.*, 2003; Madrid and Mancho, 2009) and the direct calculation of manifolds as material surfaces (Mancho *et al.*, 2003, 2004), the geodesic theory of LCS (Haller and Beron-Vera, 2012) and the variational theory of LCS (Farazmand and Haller, 2012), etc.

The dynamical system that governs the atmospheric flow is given by:

$$\dot{\mathbf{x}} = \mathbf{v}(\mathbf{x}(t),t) \;\;,\;\; \mathbf{x}(t_0) = \mathbf{x}_0\,, \tag{5}$$

where $\mathbf{x}(t;\mathbf{x}_0)$ represents the trajectory of a parcel that at time $t_0$ is at position $\mathbf{x}_0$, and $\mathbf{v}$ is the wind velocity field. Since our interest is in the time scale of stratospheric sudden warmings ($\sim 10$ days) we can assume to a good approximation that the fluid parcels evolve adiabatically. Therefore trajectories are constrained to surfaces of constant specific potential temperature (isentropic surfaces). We will concentrate on the 850 K surface, which is in the middle stratosphere and approximately corresponds to the10 hPa levels. In section 3 we expand on the reasons for this choice.

Nonlin. Processes Geophys. Discuss., doi:10.5194/npg-2016-81, 2016
Manuscript under review for journal Nonlin. Processes Geophys.
Published: 14 December 2016
© Author(s) 2016. CC-BY 3.0 License.

Nonlinear Processes in Geophysics
Discussions
Open Access
EGU

To compute fluid parcels trajectories it is necessary to integrate (5). As the velocity field is provided on a discrete spatio-temporal grid, the first issue to deal with is that of interpolation. We use bicubic interpolation in space and third-order Lagrange polynomials in time (see Mancho *et al.* (2006a) for details). Moreover for the time evolution we have used an adaptive Cash-Karp method. It is important to remark that as done in (de la Cámara *et al.*, 2012) for the computation of particle trajectories we use cartesian coordinates in order to avoid the singularity problem arising at the poles from the description of the Earth's system in spherical coordinates.

Our choice of LD is the function $M$ introduced in Madrid and Mancho (2009); Mendoza and Mancho (2010). The $M$ function is defined as follows:

$$M(\mathbf{x}_0, t_0, \tau) = \int_{t_0-\tau}^{t_0+\tau} ||\mathbf{v}(\mathbf{x}(t;\mathbf{x}_0), t)||\, dt\ , \tag{6}$$

where $||\cdot||$ stands for the modulus of the velocity vector. At a given time $t_0$, the function $M(\mathbf{x}_0, t_0, \tau)$ measures the arc length traced by the trajectory starting at $\mathbf{x}_0 = \mathbf{x}(t_0)$ as it evolves forwards and backwards in time for a time interval $\tau$. Sharp changes of $M$ values (what we call singular features of $M$) occur in narrow gaps and highlight stable and unstable manifolds (repelling and attracting LCS) and, at their crossings, hyperbolic trajectories. A thorough explanation of how $M$ highlights manifolds is discussed in (Mendoza and Mancho, 2010; Mancho *et al.*, 2013; Lopesino *et al.*, 2017). The capability of $M$ and its generalizations (Lagrangian Descriptors) for revealing Lagrangian coherent structures was extensively analyzed and tested in Mancho *et al.* (2013). Lopesino *et al.* (2015) and Lopesino *et al.* (2017) have recently established a rigorous mathematical foundation (in specific examples) for LDs in discrete and time continuous dynamical systems, respectively, and highlighted the underlying connections with the classical theory of dynamical systems. Lagrangian descriptors have been applied in a variety of geophysical contexts. For example, in the ocean they have been used to analyze the structure of the Kuroshio current (Mendoza and Mancho, 2012), to discuss the performance of different oceanic datasets (Mendoza *et al.*, 2014), to analyze and develop search and rescue strategies at sea (Garcia-Garrido *et al.*, 2015) and also to manage efficiently in real-time the environmental impact of marine oil spills (Garcia-Garrido *et al.*, 2016). In the field of atmospheric sciences, LDs have been used to study transport processes across the Southern SPV and RWB by de la Cámara *et al.* (2012, 2013); Smith and McDonald (2014); Guha *et al.* (2016) and to investigate the Northern Hemisphere major stratospheric final warming in 2016 (Manney and Lawrence, 2016).

As an example relevant to the case that motivates the present study, we show in Fig. 1 the evaluation of $M$ over the Southern Hemisphere using $\tau = 15$ on the 850 K isentropic level for the 5th August 2002. The representation shows a stereographic projection (see Snyder (1987)) in which the SPV is clearly visible by the bright yellow color, and also the filamentation phenomena ejecting material both from the outer and inner part of the jet. These filaments are related to the presence of hyperbolic trajectories highlighted in the figure. All figures presenting $M$ in what follows were computed with $\tau = 15$.

Nonlin. Processes Geophys. Discuss., doi:10.5194/npg-2016-81, 2016
Manuscript under review for journal Nonlin. Processes Geophys.
Published: 14 December 2016
© Author(s) 2016. CC-BY 3.0 License.

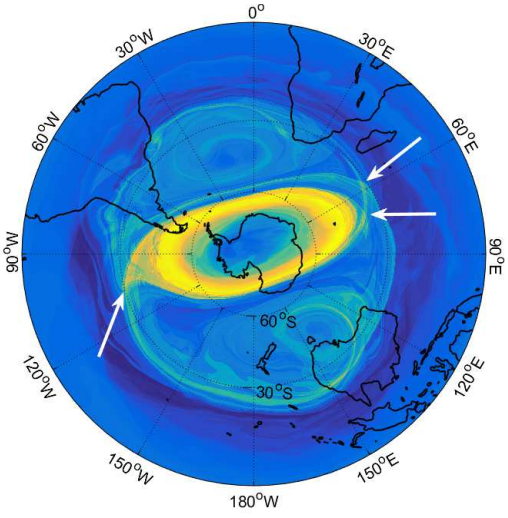


**Figure 1.** Stereographic projection of Lagrangian descriptors evaluated using $\tau = 15$ on the 850 K isentropic level for the 5th August 2002 at 00:00:00 UTC. The SPV is clearly visible as well as three hyperbolic trajectories (HTs) outside the vortex (marked with white arrows), two northeast and one southwest of it. Filamentation phenomena, which occurs in the neighborhood of HTs, is visible both inside and outside the vortex, where the outer filamentous structures play the role of eroding the jet barrier. Notice also the presence of two eddy coherent structures above and below the SPV.

## 3 Data Analysis

As we explained in the previous section, in order to characterize the planetary waves that propagate in the stratosphere we carry out a Fourier decomposition of the geopotential height. In Fig. 2 we show the axisymmetric mean-flow and waves 1 and 2 in the geopotential field for the 22nd September 2002 on the 10 hPa pressure surface. The time evolution of these waves is also described in the supplementary movies S1-S4. Animations S1-S3 contain simulations of components 0, 1 and 2 separately for the time period of interest, and S4 shows the evolution of the three waves summed. It is important to remark that, since the geopotential provides a good approximation of the streamfunction of the large-scale flow in the extratropical regions (see e.g. Holton (2004)), its analysis will help us to build in the next section a simple kinematic model.

On the 10 hPa pressure level, the winter SPV in the Southern Hemisphere is defined by a circumpolar westerly jet. During September 2002, this circulation was severely disrupted in the middle stratosphere. Figure 3a) illustrates this disruption by showing a time series of the amplitude of the axisymmetric Fourier component (see figure 2b)) of the geopotential height along a chosen longitude (as it is axisymmetric all longitudes provide the same output). This component is the most representative of the flow. In the quasi-geostrophic approximation, the latitudinal gradient of this component approximates the zonal mean velocity (Holton, 2004). The time series in figure 3a) shows that in the neighbourhood of the South Pole (between latitudes -65 to -90) this gradient changes sign around the 22nd of September 2002, indicating a reversal of the zonal meanflow.

Nonlin. Processes Geophys. Discuss., doi:10.5194/npg-2016-81, 2016
Manuscript under review for journal Nonlin. Processes Geophys.
Published: 14 December 2016
© Author(s) 2016. CC-BY 3.0 License.

Nonlinear Processes in Geophysics
Discussions
Open Access
EGU

Planetary waves in the southern stratosphere were very active during the period where the 2002 SSW developed. Fig. 3 b) illustrates the time evolution of the ratio between the amplitudes of waves 1 and 2. Increased wave 1 amplitude results in a displacement of the SPV vortex from a circumpolar configuration, while increased wave 2 results in a stretching the SPV in one direction and contraction in the orthogonal direction. According to Fig. 3 b), the amplitude of wave 1 was generally larger than that of wave 2 during the entire period, confirming the major role of this wave.

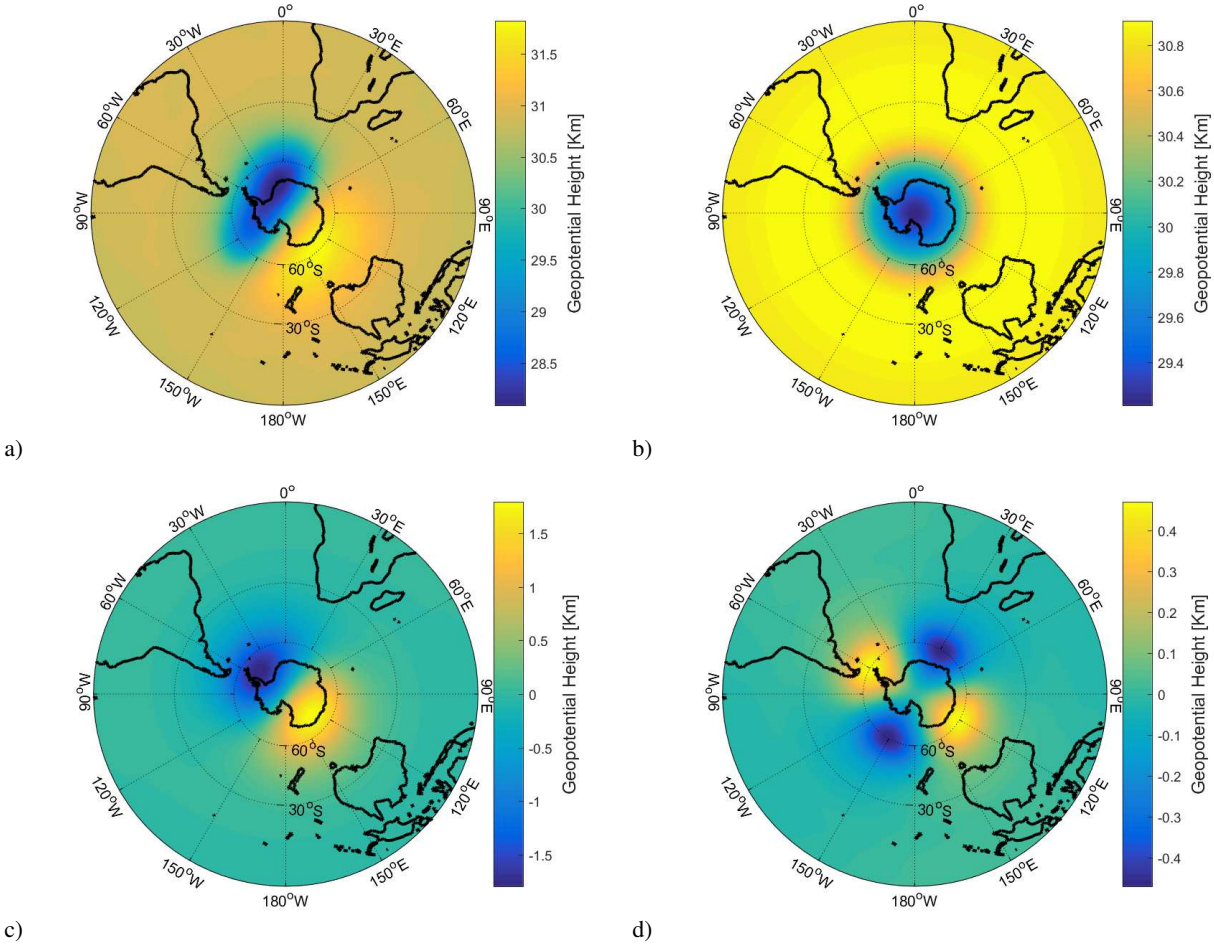


**Figure 2.** Stereographic projection of the geopotential height field and its Fourier decomposition for the 10 hPa pressure level on the 22nd September 2002 at 00:00:00 UTC: a) Geopotential height; b) Mean flow; c) Fourier component $\mathcal{Z}_1$; d) Fourier component $\mathcal{Z}_2$. Observe how the planetary wave with wavenumber 1 energetically dominates $\mathcal{Z}_2$, since its amplitude is at least three times larger.

The contribution of these different waves to the evolution of the SPV and their transport implications is clearly observed in movie S5. A regime giving rise to the stretching of material lines and the appearance of hyperbolic regions and the associated filamentation processes is observed. These filamentous structures and HTs are clearly highlighted by the application of LDs to the wind fields, as shown in Figs. 1 and 4. Filamentation phenomena occurs both inside and outside the vortex, where the outer

Nonlin. Processes Geophys. Discuss., doi:10.5194/npg-2016-81, 2016
Manuscript under review for journal Nonlin. Processes Geophys.
Published: 14 December 2016
© Author(s) 2016. CC-BY 3.0 License.

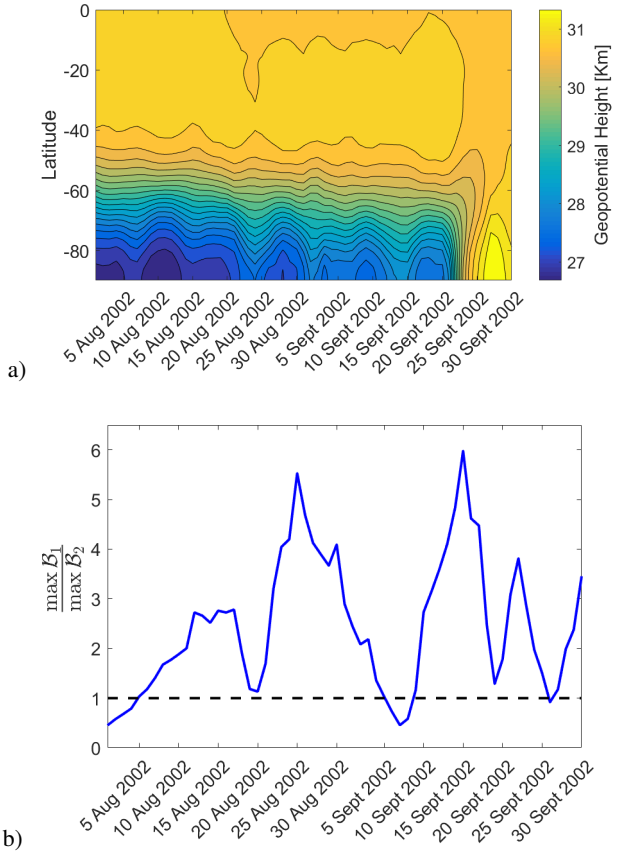


**Figure 3.** a) Time evolution of the geopotential height corresponding to the mean flow measured along a meridian. Notice the change in wind direction from westerly to easterly that takes place from the 22nd to the 24th of September 2002 giving rise to the pinching of the SPV. b) Time series of the ratio of the maximum amplitudes of Rossby waves 1 and 2. It is important to remark how the component 1 clearly dominates component 2 throughout most of the period.

Nonlin. Processes Geophys. Discuss., doi:10.5194/npg-2016-81, 2016
Manuscript under review for journal Nonlin. Processes Geophys.
Published: 14 December 2016
© Author(s) 2016. CC-BY 3.0 License.

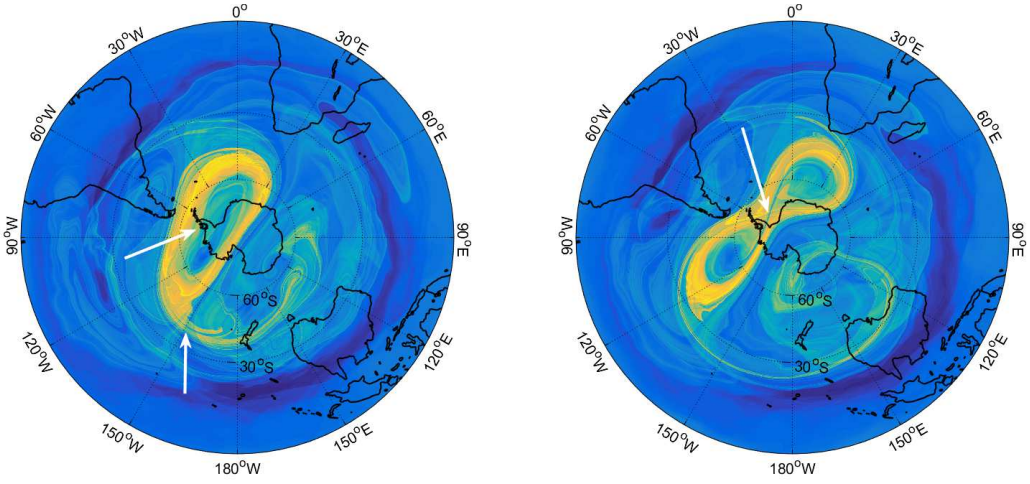


**Figure 4.** Stereographic projection of the $M$ function calculated using $\tau = 15$ on the 850 K isentropic level for the: a) 22nd September 2002 at 00:00:00 UTC; b) 24th September 2002 at 00:00:00 UTC. Filamentation phenomena and hyperbolic trajectories (marked with white arrows) are nicely captured in these simulations both in the exterior and the exterior of the SPV. Observe how the breakdown of the vortex on the 24th September occurs via the appearance of an hyperbolic point inside the polar jet which allows the transport and mixing of air across the coherent barrier.

filamentous structures play the role of eroding the jet material barrier. Also, the presence of HTs in the flow (see captions of Figs. 1 and 4) indicate regions subjected to intense deformation and mixing (see Ottino (1989)). It is important to highlight that HTs appear both inside and outside the SPV. Finally, the breakup of the SPV on the 24th September 2002 depicted in Fig. 4 b) (see also animation S5) is caused by the formation of a HT in the interior of the vortex whose manifolds connect the interior and the exterior of the jet, allowing for the interchange of air through the barrier. The pinching of the SPV takes place off the pole since the intensity of $\mathcal{Z}_1$ is dominant in the days preceding the breakup. As we approach the 24th September, $\mathcal{Z}_2$ becomes of the same order as $\mathcal{Z}_0$, and the jet elongates and flattens. At this point, the mean flow reversal is crucial for completing the pinching process and the appearance of a HT in the interior of the vortex which splits it apart.

## 4 The kinematic model

Kinematic models have a long history in the geophysical fluid dynamics community. They allow for a detailed parametric study of the influence of identified flow structures on transport and exchange of fluid parcels. All early studies utilizing the dynamical systems approach for understanding Lagrangian transport and exchange associated with flow structures such as meandering jets and travelling waves have employed kinematic models. A review of this earlier work, can be found in Samelson and Wiggins (2006).

Nonlin. Processes Geophys. Discuss., doi:10.5194/npg-2016-81, 2016
Manuscript under review for journal Nonlin. Processes Geophys.
Published: 14 December 2016
© Author(s) 2016. CC-BY 3.0 License.

Nonlinear Processes in Geophysics
Discussions
Open Access
EGU

Continuing in this spirit, in this section we propose a kinematic model that allows us to identify in a controlled fashion, the characteristics of the distinct propagating waves that are responsible for the different Lagrangian features observed in the SPV. Our kinematic model is inspired by the Fourier component decomposition of the geopotential extracted from the ECMWF data as discussed in the previous section. The analysis of data from August and September 2002 shows a mean axisymmetric flow, disturbed mainly by waves with planetary wavenumbers 1 and 2 whose amplitudes and phase speeds vary in a time-dependent fashion.

Therefore we propose a kinematic model in the form of a streamfunction that is the sum of the first three Fourier components of the geopotential field:

$$\Psi = \varepsilon_0 \Psi_0 + \varepsilon_1 \Psi_1 + \varepsilon_2 \Psi_2 \,, \tag{7}$$

where $\varepsilon_0, \varepsilon_1, \varepsilon_1$ are the perturbation parameters and $\Psi_i$ are the Fourier components along the azimuthal direction with wavenumbers $i = 0, 1, 2$ respectively, which we describe next.

The streamfunction is defined on a horizontal plane $(x, y)$ that is the orthographic projection of the Southern hemisphere onto the equatorial plane (cf. Snyder (1987)). For simplicity, and in order to highlight the periodicity along the azimuthal direction, the components of the streamfunction are given in terms of polar coordinates satisfying $x = r\cos(\lambda)$ and $y = r\sin(\lambda)$ where the azimuthal direction $\lambda$ is related to the geographical longitude. and $r$ is related to the geographical latitude.

The mean axisymmetric flow is given by:

$$\Psi_0 = e^{-r}(ar + a - r(r+2) - 2) \tag{8}$$

where $a$ is a tunable constant that is varied to represent different phenomena. This component of the streamfunction has been computed by modeling the velocity in the azimuthal direction as $v_\lambda = r(r-a)e^{-r}$ and then integrating with respect to $r$. The other streamfunction components are:

$$\Psi_1 = -r^2 e^{-r^2} \sin(\lambda) \tag{9}$$

and

$$\Psi_2 = (r/d)^2 e^{-r^2/d} \sin(2\lambda) \tag{10}$$

where $d$ is also a tunable constant. A representation of the Fourier components of the streamfunction is given in figure 5.

The components $\Psi_1$ and $\Psi_2$ typically are time dependent because they are waves that propagate in the azimuthal direction $\lambda$. In our setting we just consider the propagation of wave two, thus expression (10) is rewritten as follows:

$$\Psi_2 = (r/d)^2 e^{-r^2/d} \sin(2(\lambda + 2\omega_2 t)). \tag{11}$$

Nonlin. Processes Geophys. Discuss., doi:10.5194/npg-2016-81, 2016
Manuscript under review for journal Nonlin. Processes Geophys.
Published: 14 December 2016
© Author(s) 2016. CC-BY 3.0 License.

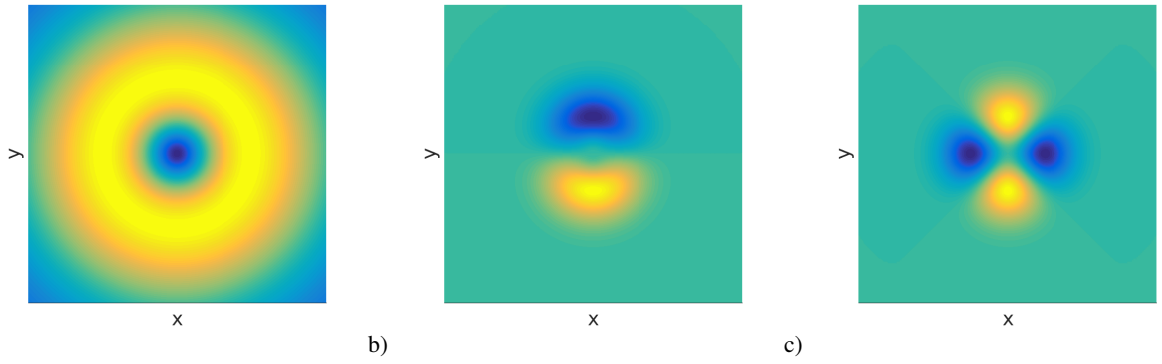


**Figure 5.** Representation of the three components of the streamfunction. a) $\varepsilon_0 \Psi_0$, for $a = 2$ and $\varepsilon_0 < 0$; b) $\Psi_1$; c) $\Psi_2$ for $d = 1$.

Additionally the amplitudes $\varepsilon_1$ and $\varepsilon_2$ are time dependent as they switch on and off the presence of each wave:

$$\varepsilon_1 = \eta_1(1+\sin(\mu t+\pi)),\ \varepsilon_2 = \eta_2(1+\sin(\mu t)). \tag{12}$$

Here $\eta_1$ and $\eta_2$ are constants. The time dependence of $\varepsilon_1$ and $\varepsilon_2$ allows us to analyze each wave and their transient effect on the observed Lagrangian structures and therefore their transport implications. The time dependence in (12) is such that one amplitude decreases when the other increases, roughly allowing conservation of the total energy when both waves are present. In the simulations presented below $\mu = 2\pi/10$.

The equations of motion for fluid parcels in the Cartesian coordinates $(x, y)$ are given by Hamilton's equations:

$$\frac{dx}{dt} = -\frac{\partial \Psi}{\partial y},\ \frac{dy}{dt} = \frac{\partial \Psi}{\partial x} \tag{13}$$

Figure 6 summarizes the Lagrangian findings obtained from the kinematic model with different parameters. Figures 6 a) and b) highlight a jet which in the interior is eroded, respectively, by the presence of perturbing waves with wave numbers 1 or 2. In a) the parameters switch on a transient amplitude for wave 1 ($\eta_1 = 1, \eta_2 = 0$) on an axisymmetric flow where $\varepsilon_0 = 2.5$ and $a = 0.5$. Lagrangian structures are obtained from the function $M$ for $\tau = 15$. A protruding material filament from the interior of the vortex is observed, which is related to the presence of one hyperbolic trajectory. In b) parameters switch on a transient amplitude for a traveling wave 2 ($\eta_1 = 0, \eta_2 = 1$) and constants $d = 2$ and $\omega_2 = -\pi/25$ on an axisymmetric flow where $\varepsilon_0 = 2.6$ and $a = 0.75$. Here also $\tau = 15$. Two filaments projecting material from the interior of the vortex are observed, and they are related to the presence of two hyperbolic trajectories. The interior filaments recover features that are identified as interior Rossby wave breaking phenomena in de la Cámara *et al.* (2013); Guha *et al.* (2016) and are also visible from the reanalysis data as shown in Figures 1 and 4a).

Figures 6 c) and d) display a jet eroded in its outer part by perturbing waves with wave number 1 or 2. In c) parameters switch on a transient amplitude for wave 1 ($\eta_1 = 1, \eta_2 = 0$) on an axisymmetric flow in which $\varepsilon_0 = -2.5$ and $a = 2$. Lagrangian

Nonlin. Processes Geophys. Discuss., doi:10.5194/npg-2016-81, 2016
Manuscript under review for journal Nonlin. Processes Geophys.
Published: 14 December 2016
© Author(s) 2016. CC-BY 3.0 License.

Nonlinear Processes in Geophysics
Discussions
Open Access
EGU

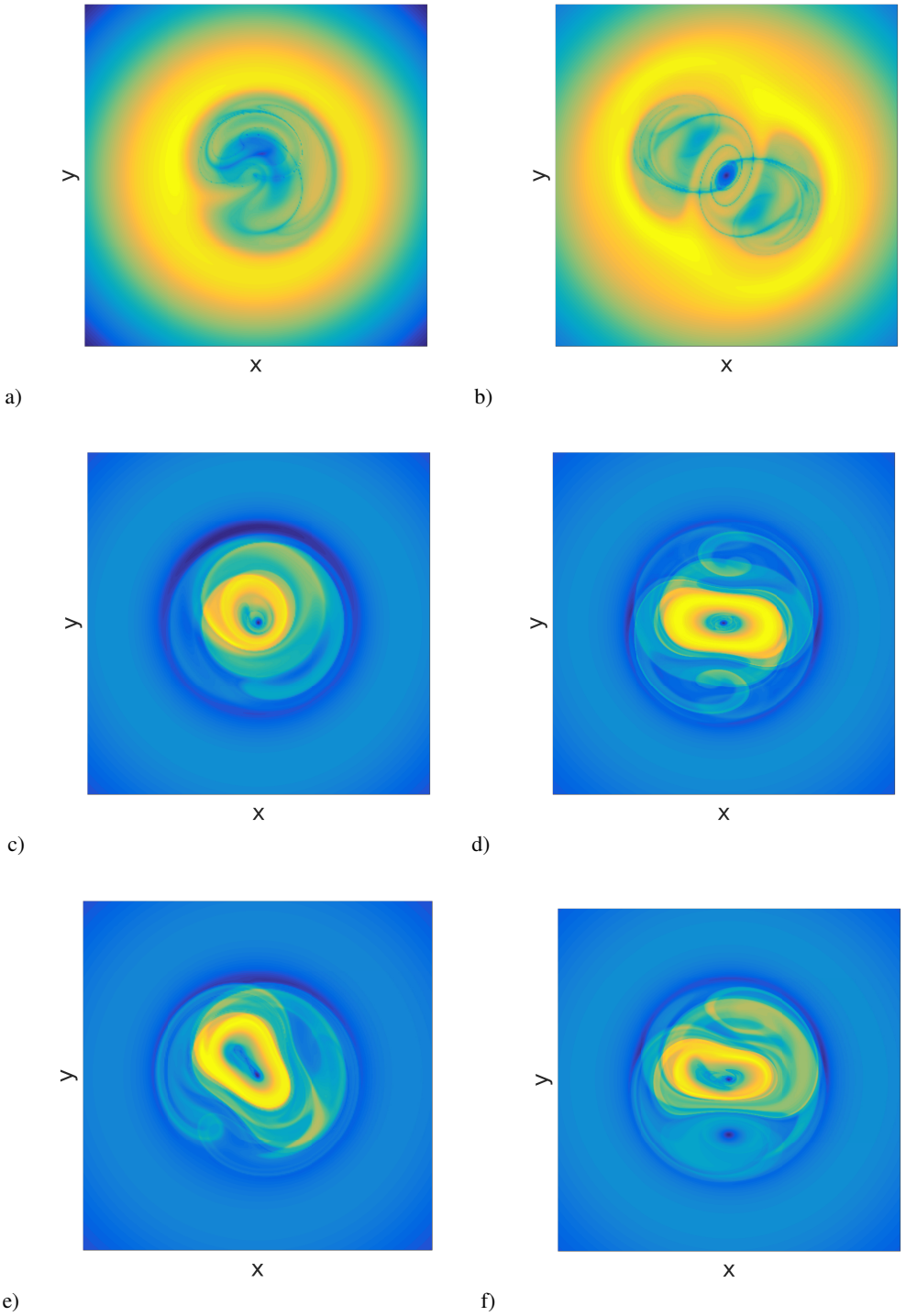


**Figure 6.** Lagrangian patterns obtained for $\tau = 15$ and different parameter settings in the kinematic model. a) The model keeps $\Psi_0$ and $\Psi_1$ adjusted to perturb the vortex in its interior part; b) the model keeps $\Psi_0$ and $\Psi_2$ adjusted to perturb the vortex in its interior part; c) Fourier components $\Psi_0$ and $\Psi_1$ the latter adjusted to perturb the vortex in its outer part; d) Fourier components $\Psi_0$ and $\Psi_2$ the latter adjusted to perturb the vortex in its outer part; e) the model keeps $\Psi_0$, $\Psi_1$ and $\Psi_2$; f) the model keeps $\Psi_0$, $\Psi_1$ and $\Psi_2$ with parameters adjusted differently to e).

Nonlin. Processes Geophys. Discuss., doi:10.5194/npg-2016-81, 2016
Manuscript under review for journal Nonlin. Processes Geophys.
Published: 14 December 2016
© Author(s) 2016. CC-BY 3.0 License.

Nonlinear Processes in Geophysics
Discussions
Open Access
EGU

structures are obtained from the function $M$ for $\tau = 15$. One hyperbolic trajectory at the outer boundary of the jet is observed ejecting material of the vortex. In d) the parameters switch on a transient amplitude for a non travelling ($\omega_2 = 0$) wave 2 ($\eta_1 = 0, \eta_2 = 1$) and constant $d = 1$ on an axisymmetric flow in which $\varepsilon_0 = -2.5$ and $a = 2$. Here also $\tau = 15$ and two hyperbolic trajectories are visible in the external jet boundary. The filaments ejecting material in the outer part have close connections to those present in Figures 1 and 4a) that have been related to Rossby wave breaking phenomena at midlatitudes.

Figures 6 e) and f) show a jet which is perturbed by waves with wave numbers 1 and 2. In e) the parameters are $\eta_1 = 1$, $\eta_2 = 1$, $d = 1$ and $\omega_2 = \pi/30$, representing a transient amplitude for wave one and a transient amplitude for a travelling wave two, on an axisymmetric flow in which $\varepsilon_0 = -2.5$ and $a = 2$. In f) the parameters are $\eta_1 = 1, \eta_2 = 1$ with $d = 1$ and $\omega_2 = 0$, representing a transient amplitude for wave one and a transient amplitude for a non travelling wave two, on an axisymmetric flow in which $\varepsilon_0 = -2.5$ and $a = 2$ . The patterns are obtained for $\tau = 15$. The filamentous structures and jet shape greatly resemble those present in the reanalysis data as shown in Figures 1 and 4a).

Figure 4b) shows the pinching of the SPV on the 24th September 2002 before its breakup. From the kinematic point of view the pinching is justified by the dominant presence of $\Psi_2$. However the fact that the main jet in Figure 4b) is not centered in the South pole, indicates also the presence of a component $\Psi_1$. Figure 7 shows the Lagrangian patterns obtained for a non travelling ($\omega_2 = 0$), fixed amplitude ( $\eta_2 = 4$, $\mu = 0$) wave 2 with $d = 1$ overlapped with the axisymmetric mean flow obtained with $\varepsilon_0 = 1$ and $a = 0.1$, where the pinching effect is visible. The two vortices at the top and at the bottom of the pinching point would be balanced if component $\Psi_1$ were present. The reversal of the axisymmetric flow described in Section 3 during the observed pinching event is in agreement with the decreasing amplitude of $\Psi_0$ (change of sign implies approaching to zero) and dominance of component 2.

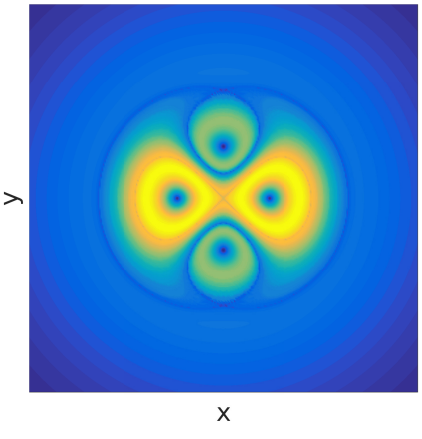


**Figure 7.** The function $M$ evaluated on a stationary velocity field obtained for a stationary non transient wave two, $\eta_2 = 4$, $\omega_2 = 0$, $\mu = 0$ and $d = 1$ overlapped with $\Psi_0$, $a = 0.1$ and $\varepsilon_0 = 1$.

Nonlin. Processes Geophys. Discuss., doi:10.5194/npg-2016-81, 2016
Manuscript under review for journal Nonlin. Processes Geophys.
Published: 14 December 2016
© Author(s) 2016. CC-BY 3.0 License.

Nonlinear Processes in Geophysics
Discussions
Open Access
EGU

## 5 Kinematic models and conservation of Potential Vorticity

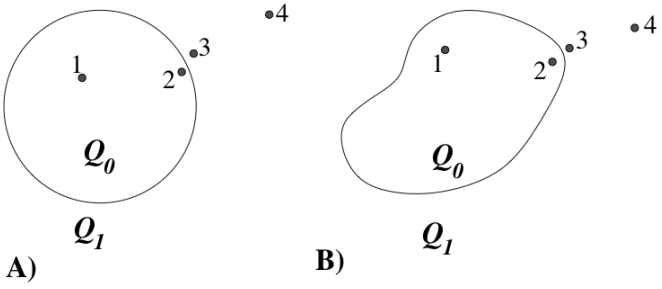


**Figure 8.** Evolution of a vorticity patch. a) Initial vorticity distribution at time $t_0$; b) Evolution of the domain with constant vorticity at time $t_1$.

In this section we discuss the connection between the kinematic model introduced in the previous section and a fundamental dynamical principle of geophysical fluids. Geophysical flows that are adiabatic and frictionless conserve the potential vorticity $Q$ along trajectories. Conservation of $Q$ is expressed as follows:

$$\frac{dQ}{dt} = 0 \tag{14}$$

Here $d/dt$ stands for the material derivative. A natural question here is to discuss a setting in which a proposed kinematic model would conserve $Q$.

Rossby wave breaking phenomena have been studied in simplified dynamical models by Polvani and Plumb (1992); Nakamura and Plumb (1994). These works have considered the quasigeostrophic motion of simple vortices in a shallow water system which is perturbed by topographically driven Rossby waves. Polvani and Plumb (1992) describe a setting in which $Q$ is given by:

$$Q = f_0 + \nabla^2\Psi - \gamma^2\Psi + f_0\frac{h}{D} \tag{15}$$

Here $f_0$ is a constant related to the rotation rate, $D$ is the mean depth of the shallow water system, $D-h$ is the total depth, $h$ is the bottom topography which is small when compared to $D$, and $\gamma = f_0/\sqrt{g_0 D}$, where $g_0$ is the gravity constant. $\Psi$ is the geostrophic streamfunction for the horizontal velocity field.

Given a vorticity distribution $Q$ at an initial time, the dynamical approach computes velocities by inverting Eq. (15) for $\Psi$ and solving the resulting equation by means of a contour dynamics algorithm (Dritschel, 1989). In the kinematic approach the field $\Psi$ is given and we seek conditions for which Eqs. (14)-(15) hold. A first start in this discussion is to consider an initial $Q$ distribution which consists of a constant $Q_0$ value in the whole domain and which is kept like that for all time. In this case any fluid parcel trajectory will straightforwardly satisfy Eq. (14), as while it moves $Q$ does not change in the domain. On the other hand, if $\Psi$ and (constant) $Q$ are specified, then Eq. (14) and Eq. (15) hold with appropriately chosen $h$.

Nonlin. Processes Geophys. Discuss., doi:10.5194/npg-2016-81, 2016
Manuscript under review for journal Nonlin. Processes Geophys.
Published: 14 December 2016
© Author(s) 2016. CC-BY 3.0 License.

Nonlinear Processes in Geophysics Discussions
Open Access
EGU

Now we ask about other not so simple initial distributions of $Q$, that also satisfy Eqs. (14)-(15). The initial potential vorticity distribution discussed by Polvani and Plumb (1992) is illustrated in Figure 8 a). They consider a simple circular patch of constant value $Q_0$ in a domain $P$, surrounded by a region with also constant vorticity $Q_1 < Q_0$. This initial distribution, in our particular setting would clearly satisfy Eq. (14) for fluid parcels inside each region $Q_0$ and $Q_1$ if the evolution from time $t_0$ to time $t_1 = t_0 + \Delta t$ keeps fluid parcels inside each region. Fluid parcels close to the boundary at $t_0$ would not have a problem preserving $Q$ if the domain $P$ at $t_1$ is distorted according to the equations of motion Eq. (13) for the prescribed $\Psi$. Figure 8 b) illustrates the evolution of the domain $P$ at time $t_1$ and the position of fluid parcels labelled as 1,2,3 and 4 preserving vorticity. If the function $Q$ is a time dependent function defined in this way then Eq. (14) is satisfied in our setting. We also note that Eq. (15) is satisfied if $h$ is constructed from the time dependent $Q$ function and the prescribed $\Psi$ exactly as we did in the example at the beginning of this section. Finally we note that this argument can be extended to any initial distribution of $Q$ defined as a piecewise constant function. Therefore the topographic forcing $h$ is a function adjusted to preserve the conservation of the potential vorticity. Similar settings that consider a time dependent topography (physically related to a time dependent lower layer boundary) is described by Nakamura and Plumb (1994). Without this forcing, kinematic models would not preserve potential vorticity. This latter case is discussed by Samelson and Wiggins (2006).

## 6 Conclusions

In this work we propose a simple kinematic model for studying transport phenomena in the Antarctic Polar vortex. We are interested in gaining insights into the processes which carry material outwards from the vortext structure and inwards to the vortex structure.

The construction of the kinematic model is realized by analyzing geopotential height data produced by the ECMWF. In particular our focus is on the stratospheric sudden warming event that took place in 2002, producing the pinching and then breaking of the stratospheric polar vortex. We identify the prevalent Fourier components during this period, which consist of a mean axisymmetric flow and waves with wavenumbers one and two. The kinematic model is based on analytical expressions which recover the spatial structures of these representative Fourier components. The model can be controlled so that waves with wavenumbers one and two can be switched on and off independently. We are also able to adjust the relative position of the waves with respect to the mean axisymmetric flow.

The study of Lagrangian transport phenomena in the ERA-Interim reanalysis data by means of Lagrangian Descriptors highlight hyperbolic trajectories in the outer and inner part of vortex. These trajectories are the Lagrangian objects that cause filamentation phenomena. The Lagrangian study of the kinematic model sheds light on the role played by waves in this regard. We find that the model with just wave one, produces just one hyperbolic trajectory that can erode material either from the interior (Fig. 6 a)) or exterior (Fig. 6 c)) part of the jet, depending on its relative position to it. Similarly the model with just wave two, produces two hyperbolic trajectories eroding material either from the interior (Fig. 6 b)) or exterior (Fig. 6 d)) part of the jet, depending on its relative position. The presence of waves one and two produce complex Lagrangian patterns (Figs. 6 e) and f)) remarkably similar to those observed from the analysis of the complex reanalysis data. These results confirm the

Nonlin. Processes Geophys. Discuss., doi:10.5194/npg-2016-81, 2016
Manuscript under review for journal Nonlin. Processes Geophys.
Published: 14 December 2016
© Author(s) 2016. CC-BY 3.0 License.



findings discussed by Guha *et al.* (2016). Finally we point out that our analysis shows that the breaking of the polar vortex is justified by the sudden growth of waves one and two and the decay and change of direction of the axisymmetric flow.

*Acknowledgements.* V. J. García-Garrido, J Curbelo and A. M. Mancho are supported by MINECO grant MTM2014-56392-R. The research of C. R. Mechoso is supported by the U.S. NSF grant AGS-1245069. The research of S. Wiggins is supported by ONR grant No. N00014-01-1-0769. We also acknowledge support from ONR grant No. N00014-16-1-2492.

Nonlin. Processes Geophys. Discuss., doi:10.5194/npg-2016-81, 2016
Manuscript under review for journal Nonlin. Processes Geophys.
Published: 14 December 2016
© Author(s) 2016. CC-BY 3.0 License.



## References

Aurell, E., Boffeta, G., Crisanti, A., Paladin, G., and Vulpiani, A. (1997). Predictability in the large: An extension of the concept of Lyapunov exponent. *J. Phys. A :Math. Gen.*, **30**, 1–26.

Bower, A. S. (1991). A simple kinematic mechanism for mixing fluid parcels across a menadering jet. *J. Phys. Oceanogr.*, **21**, 173–180.

Bowman, K. P. (1993). Large-scale isentropic mixing properties of the Antarctic polar vortex from analyzed winds. *Journal of Geophysical Research*, **98**, 23013–23027.

Bowman, K. P. (2006). Transport of carbon monoxide from the tropics to the extratropics. *Journal of Geophysical Research: Atmospheres*, **111**(D2).

Charlton, A. J., O'Neill, A., Lahoz, W. A., and Berrisford, P. (2006). The splitting of the stratospheric polar vortex in the southern hemisphere, september 2002: Dynamical evolution. *J. Atmos. Sci.*, **66**, 590–602.

de la Cámara, A., Mancho, A. M., Ide, K., Serrano, E., and Mechoso, C. (2012). Routes of transport across the Antarctic polar vortex in the southern spring. *J. Atmos. Sci.*, **69**(2), 753–767.

de la Cámara, A., Mechoso, R., Mancho, A. M., Serrano, E., and Ide., K. (2013). Isentropic transport within the Antarctic polar night vortex: Rossby wave breaking evidence and Lagrangian structures. *J. Atmos. Sci.*, **70**, 2982–3001.

Dee, D. P. *et al.* (2011). The ERA-Interim reanalysis: configuration and performance of the data assimilation system. *Quarterly Journal of the Royal Meteorological Society*, **137**(656), 553–597.

Dritschel, D. G. (1989). Contour dynamics and contour surgery: numerical algorithms for extended, high-resolution modelling of vortex dynamics in two-dimensional, inviscid, incompressible flows. *Comput. Phys. Rep.*, **10**, 77–146.

Farazmand, M. and Haller, G. (2012). Computing Lagrangian Coherent Structures from variational LCS theory. *Chaos*, **22**, 013128.

Garcia-Garrido, V. J., Mancho, A. M., and Wiggins, S. (2015). A dynamical systems approach to the surface search for debris associated with the disappearance of flight MH370. *Nonlin. Proc. Geophys.*, **22**, 701–712.

Garcia-Garrido, V. J., Ramos, A., Mancho, A. M., Coca, J., and Wiggins, S. (2016). A dynamical systems perspective for a real-time response to a marine oil spill. *Marine Pollution Bulletin.*, pages 1–10.

Guha, A., Mechoso, C. R., Konor, C. S., and Heikes, R. P. (2016). Modeling rossby wave breaking in the southern spring stratosphere. *J. Atmos. Sci.*, **73**(1), 393–406.

Haller, G. (2000). Finding finite-time invariant manifolds in two-dimensional velocity fields. *Chaos*, **10**(1), 99–108.

Haller, G. (2001). Distinguished material surfaces and coherent structures in three-dimensional fluid flows. *Physica D*, **149**, 248–277.

Haller, G. and Beron-Vera, F. J. (2012). Geodesic theory of transport barriers in two-dimensional flows. *Physica D*, **241**(7), 1680–1702.

Haller, G. and Yuan, G. (2000). Lagrangian coherent structures and mixing in two-dimensional turbulence. *Physica D*, **147**, 352–370.

Holton, J. R. (2004). *An Introduction to Dynamic Meteorology*. Elsevier Academic Press.

Ide, K., Small, D., and Wiggins, S. (2002). Distinguished hyperbolic trajectories in time dependent fluid flows: analytical and computational approach for velocity fields defined as data sets. *Nonlin. Proc. Geophys.*, **9**, 237–263.

Ju, N., Small, D., and Wiggins, S. (2003). Existence and computation of hyperbolic trajectories of aperiodically time-dependent vector fields and their approximations. *Int. J. Bif. Chaos*, **13**, 1449 –1457.

Juckes, M. N. and McIntyre, M. E. (1987). A high-resolution one-layer model of breaking planetary waves in the stratosphere. *Nature*, **328**, 590–596.

Nonlin. Processes Geophys. Discuss., doi:10.5194/npg-2016-81, 2016
Manuscript under review for journal Nonlin. Processes Geophys.
Published: 14 December 2016
© Author(s) 2016. CC-BY 3.0 License.

Krüger, K., Naujokat, B., and Labitzke, K. (2005). The unusual midwinter warming in the southern hemisphere stratosphere 2002: A comparison to northern hemisphere phenomena. *J. Atmos. Sci.*, **62**, 603–613.

Lopesino, C., Balibrea-Iniesta, F., Wiggins, S., and Mancho, A. M. (2015). Lagrangian descriptors for two dimensional, area preserving autonomous and nonautonomous maps. *Communications in Nonlinear Science and Numerical Simulations*, **27**(1-3), 40–51.

Lopesino, C., Balibrea-Iniesta, F., García-Garrido, V. J., Wiggins, S., and Mancho, A. M. (2017). A theoretical framework for lagrangian descriptors. to appear. *International Journal of Bifurcation and Chaos.*

Madrid, J. A. J. and Mancho, A. M. (2009). Distinguished trajectories in time dependent vector fields. *Chaos*, **19**, 013111.

Malhotra, N. and Wiggins, S. (1998). Geometric structures, lobe dynamics, and Lagrangian transport in flows with aperiodic time-dependence, with applications to Rossby wave flow. *J. Nonlinear Science*, **8**, 401–456.

Mancho, A. M., Small, D., Wiggins, S., and Ide, K. (2003). Computation of Stable and Unstable Manifolds of Hyperbolic Trajectories in Two-Dimensional, Aperiodically Time-Dependent Vectors Fields. *Physica D*, **182**, 188–222.

Mancho, A. M., Small, D., and Wiggins, S. (2004). Computation of hyperbolic trajectories and their stable and unstable manifolds for oceanographic flows represented as data sets. *Nonlin. Proc. Geophys.*, **11**, 17–33.

Mancho, A. M., Small, D., and Wiggins, S. (2006a). A comparison of methods for interpolating chaotic flows from discrete velocity data. *Computers and Fluids*, **35**, 416–428.

Mancho, A. M., Small, D., and Wiggins, S. (2006b). A tutorial on dynamical systems concepts applied to Lagrangian transport in oceanic flows defined as finite time data sets: Theoretical and computational issues. *Phys. Rep.*, **237**(3-4), 55–124.

Mancho, A. M., Wiggins, S., Curbelo, J., and Mendoza, C. (2013). Lagrangian descriptors: A method for revealing phase space structures of general time dependent dynamical systems. *Communications in Nonlinear Science and Numerical Simulations*, **18**(12), 3530–3557.

Manney, G. L. and Lawrence, Z. D. (2016). The major stratospheric final warming in 2016: Dispersal of vortex air and termination of Arctic chemical ozone loss. *Atmospheric Chemistry and Physics Discussions*, **2016**, 1–40.

Manney, G. L., Sabutis, J. L., Alley, D. R., Lahoz, W. A., Scaife, A. A., Randall, C. E., Pawson, S., Naujokat, B., and Swinbank, R. (2006). Simulations of dynamics and transport during the september 2002 antarctic major warming. *J. Atmos. Sci.*, **66**(690-707).

McIntyre, M. E. and Palmer, T. N. (1983). Breaking planetary waves in the stratosphere. *Nature*, **305**, 593–600.

McIntyre, M. E. and Palmer, T. N. (1984). The surf zone in the stratosphere. *Journal of Atmospheric and Terrestrial Physics*, **46**(9), 825–849.

McIntyre, M. E. and Palmer, T. N. (1985). A note on the general concept of wave breaking for rossby and gravity waves. *Pure and Applied Geophysics*, **123**(6), 964–975.

Mechoso, C. R., O'Neill, A., Pope, V. D., and Farrara, J. D. (1988). A study of the stratospheric final warming of 1982 in the southern hemisphere. *Quarterly Journal of the Royal Meteorological Society*, **114**(484), 1365–1384.

Mendoza, C. and Mancho, A. M. (2010). The hidden geometry of ocean flows. *Phys. Rev. Lett.*, **105**(3), 038501.

Mendoza, C. and Mancho, A. M. (2012). The Lagrangian description of aperiodic flows: a case study of the Kuroshio Current. *Nonlin. Proc. Geophys.*, **19**(14), 449–472.

Mendoza, C., Mancho, A. M., and Wiggins, S. (2014). Lagrangian descriptors and the assesment of the predictive capacity of oceanic data sets. *Nonlin. Proc. Geophys.*, **21**, 677–689.

Morales-Juberías, R., Sayanagi, K. M., Simon, A. A., Fletcher, L. N., and Cosentino, R. G. (2015). Meandering shallow atmospheric jet as a model of saturn's north-polar hexagon. *The Astrophysical Journal Letters*, **806**, L18 (6pp).

Nakamura, M. and Plumb, R. A. (1994). The effects of flow asymmetry on the direction of rossby wave breaking. *J. Atmos. Sci.*, **51**, 2031–2044.

Nonlin. Processes Geophys. Discuss., doi:10.5194/npg-2016-81, 2016
Manuscript under review for journal Nonlin. Processes Geophys.
Published: 14 December 2016
© Author(s) 2016. CC-BY 3.0 License.

Nonlinear Processes in Geophysics
Discussions
Open Access
EGU

Ottino, J. M. (1989). *The Kinematics of Mixing: Stretching, Chaos, and Transport*. Cambridge University Press, Cambridge, England. Reprinted 2004.

Polvani, L. M. and Plumb, R. A. (1992). Rossby wave breaking, microbreaking, filamentation, and secondary vortex formation: The dynamics of a perturbed vortex. *J. Atmos. Sci.*, **49**(6), 462–476.

Rabier, F. *et al.* (2010). The concordiasi project in antarctica. *Bulletin of the American Meteorological Society*, **91**(1), 69–86.

Rypina, I. I., Brown, M. G., Beron-Vera, F. J., Kocak, H., Olascoaga, M. J., and Udovydchenkov, I. A. (2007). On the lagrangian dynamics of atmospheric zonal jets and the permeability of the stratospheric polar vortex. *J. Atmos. Sci.*, **64**, 3595–3610.

Samelson, R. and Wiggins, S. (2006). *Lagrangian Transport in Geophysical Jets and Waves: The Dynamical Systems Approach*. Springer-Verlag, New York.

Samelson, R. M. (1992). Fluid exchange across a meandering jet. *J. Phys. Oceanogr.*, **22**(4), 431–440.

Shadden, S. C., Lekien, F., and Marsden, J. E. (2005). Definition and properties of Lagrangian Coherent Structures from finite-time Lyapunov exponents in two-dimensional aperiodic flows. *Physica D*, **212**, 271–304.

Simmons, A., Uppala, S., Dee, D., and S, K. (2007). ERA-Interim: New ECMWF reanalysis products from 1989 onwards. *ECMWF Newsletter*, **110**, 25–35.

Smith, M. L. and McDonald, A. J. (2014). A quantitative measure of polar vortex strength using the function m. *J. Gephys.Res. Atmos.*, **119**, 5966–5985.

Snyder, J. P. (1987). *Map Projections–A Working Manual*. U.S. Geological Survey professional paper. U.S. Government Printing Office.

Stewartson, K. (1977). The evolution of the critical layer of a rossby wave. *Geophysical & Astrophysical Fluid Dynamics*, **9**(1), 185–200.

Warn, T. and Warn, H. (1978). The evolution of a nonlinear critical level. *Studies in Applied Mathematics*, **59**(1), 37–71.